catalysts

MDPI

Article

Optimized Synthesis Routes of MnO_x-ZrO_2 Hybrid Catalysts for Improved Toluene Combustion

Xin Huang [1], Luming Li [2,3,*], Rong Liu [4,*], Hongmei Li [2], Li Lan [5] and Weiqi Zhou [1]

1 School of Mechanical Engineering, Chengdu University, Chengdu 610106, China; huangxin@stu.cdu.edu.cn (X.H.); zhouweiqi@stu.cdu.edu.cn (W.Z.)
2 College of Food and Biological Engineering, Chengdu University, Chengdu 610106, China; lihongmei@cdu.edu.cn
3 Institute for Advanced Study, Chengdu University, Chengdu 610106, China
4 School of Preclinical Medicine (Nursing College), Chengdu University, Chengdu 610106, China
5 College of Materials and Mechatronics, Jiangxi Science and Technology Normal University, Nanchang 330013, China; lanlijxstnu@outlook.com
* Correspondence: liluming@cdu.edu.cn (L.L.); liurong02@cdu.edu.cn (R.L.)

Abstract: In this contribution, the three Mn-Zr catalysts with $Mn_xZr_{1-x}O_2$ hybrid phase were synthesized by two-step precipitation route (TP), conventional coprecipitation method (CP) and ball milling process (MP). The components, textural and redox properties of the Mn-Zr hybrid catalysts were studied via XRD, BET, XPS, HR-TEM, H_2-TPR. Regarding the variation of synthesis routes, the TP and CP routes offer a more obvious advantage in the adjustment of the concentration of $Mn_xZr_{1-x}O_2$ solid solution compared to the MP process, which directly commands the content of Mn^{4+} and oxygen vacancy and lattice oxygen, and thereby leads to the enhanced mobility of reactive oxygen species and catalytic activity for toluene combustion. Moreover, the TP-Mn2Zr3 catalyst with the enriched exposure content of 51.4% for the defective (111) lattice plane of $Mn_xZr_{1-x}O_2$ exhibited higher catalytic activity and thermal stability for toluene oxidation than that of the CP-Mn2Zr3 sample with a value of 49.3%. This new observation will provide a new perspective on the design of bimetal catalysts with a higher VOCs combustion abatement.

Keywords: Mn-Zr solid solution; toluene; active oxygen; combustion

Citation: Huang, X.; Li, L.; Liu, R.; Li, H.; Lan, L.; Zhou, W. Optimized Synthesis Routes of MnO_x-ZrO_2 Hybrid Catalysts for Improved Toluene Combustion. *Catalysts* **2021**, *11*, 1037. https://doi.org/10.3390/catal11091037

Academic Editor: Roberto Fiorenza

Received: 2 August 2021
Accepted: 25 August 2021
Published: 27 August 2021

1. Introduction

Volatile organic compounds (VOCs) have been considered important harmful pollutants and can be transferred into secondary aerogel and ozone via complex photochemical reactions in the atmosphere, which are threatening the ecological environment and human health [1–4]. It is urgent to adopt effective routes to control VOCs emissions. In particular, the toluene with toxicity and carcinogenicity is one of the most common VOCs, be discharged from the petrochemical industry, and be normally selected as the target VOCs to test the activity of catalyst.

Up to now, several techniques, such as adsorption and absorption, thermal incineration, plasma, membrane separation, biological treatment, and catalytic oxidation, have been widely reported for the degradation of VOCs [5]. Among them, catalytic oxidation has been considered one of the most promising technologies because it can completely convert VOCs under relatively low temperatures (<400 °C) into harmless CO_2 and H_2O with low energy consumption, which has gained a lot of attention either in scientific and industrial fields. The key issue of catalytic oxidation is to design catalysts with high catalytic activity and low cost [6,7].

Given the active components of the VOCs catalysts, catalysts can be divided into noble metal catalysts and non-noble metal catalysts. There is no doubt that the supported noble metal catalysts have higher activity at lower temperatures. However, the disadvantages of

noble metal catalysts also need to be taken into consideration, such as high price, scarce resources, poor thermal stability, and sulfur resistance, etc., which fades their industrial application [8–10]. Therefore, it is necessary to develop alternative catalysts with high catalytic activity. The transition metal oxides have many advantages, such as relatively low price, good activity, abundant content in the earth, and environmental friendliness, which have attracted great interest [11]. For example, manganese-based oxides have been confirmed as one of the most potential alternates to noble metal catalysts and exhibited high catalytic activity due to the high mobility of lattice oxygen and the existence of transformation of unstable valence states, such as $Mn^{4+} \leftrightarrow Mn^{3+} \leftrightarrow Mn^{2+}$ [12–15]. In addition, the physical and chemical characteristics of the catalysts, such as morphology [8,16], specific surface area [17], oxygen vacancy [18], reducibility, and reactivity of lattice oxygen [19], oxygen migration rate [14], also determine the efficiency of the catalytic oxidation of VOCs. However, it is difficult to efficiently remove certain VOCs for a single phase of MnO_x due to the poor thermal stability [12,20]. Some studies have reported that the synthesized Mn-M (M = Co [21], Cu [22], Ce [15,23], Zr [24,25]) composite metal oxides can improve catalytic activity towards VOCs abatement through the strong interaction between the parent material and the modifier. Among them, ZrO_2-based materials show excellent corrosion resistance, high stability, and ionic conductivity, and the ZrO_2-based solid solutions keep high catalytic activity [26]. For instance, MnO_x-ZrO_2 bimetal oxides catalysts present a good catalytic activity due to their excellent redox property and thermal stability [27,28].

Choudhary et al. [29] reported that the reactivity of the lattice oxygen of Mn-doped ZrO_2 catalysts depended on the Mn/Zr ratio and calcination temperature; the Mn-doped ZrO_2 (cubic) with the Mn/Zr ratio of 0.25 prepared at a calcination temperature of 600 °C processed the best methane combustion activity. Gutie'rrez-Ortiz et al. [24] reported that Mn-Zr mixed oxides exhibited better catalytic activity for 1,2-dichloroethane (DCE) and trichloroethylene (TCE) than that of pure zirconia and manganese oxide, which was attributed to the modification effects of surface acid sites coupled with the readily accessible active oxygen. Zeng et al. [30] successfully manufactured an $MnZrO_x$ catalyst with a three-dimensional microporous (3DM) structure, which hold a better reducibility and oxygen mobility, accompanied by higher Mn^{4+}/Mn^{3+} and O_β/O_α, and the special structure significantly promoted the adsorption of reactant molecules and the mobility of lattice oxygen and propane oxidation. Compared with the B-$Mn_{0.6}Zr_{0.4}$ catalyst prepared by traditional sol–gel methods, the activation energy of propane combustion on 3DM $MnZrO_x$ decreased from 156.2 kJ·mol^{-1} to 105.0 kJ·mol^{-1}. Moreover, Yang et al. synthesized a series of impurity $Mn_xZr_{1-x}O_2$ catalysts, and it was found that low-valent manganese (Mn^{2+}) can enter zirconium lattice by substituting Zr^{4+} and inducing the formation of oxygen vacancy, and its concentration hinges on the doping content, which is conducive to the activation of oxygen on the surface of Mn-doped c-ZrO_2(111) crystal plane, thereby improving the catalytic performance for toluene oxidation [31].

Recently, we found that preparation process would play a critical role in adjusting the structural properties of nanocatalysts in oxidation reaction [32,33]. Particularly, the precipitation sequence determined the structural, redox properties, and textural stability of ZrO_2-based catalysts [34]. Inspired by those points, we constructed Mn-Zr bimetal catalysts based on the controllable catalytic active centers of $Mn_xZr_{1-x}O_2$ solid solution via a modulated precipitation sequence and further evaluated the catalytic capacity of the combustion of toluene model molecules, and the synergistic effect between ZrO_2 and manganese oxide was also analyzed.

2. Results and Discussion

2.1. Material Characterization

2.1.1. XRD Analysis

The XRD patterns of the as-prepared Mn-Zr catalysts with different Mn/Zr ratios are shown in Figure 1. Obviously, the intensity and position of the characteristic peak varies with the Mn/Zr ratio and synthesized routes. The intensity of characteristic peaks

of $Mn_xZr_{1-x}O_2$ solid solution was increased as the Mn/Zr ratio decreased, in which the diffraction peaks located at 30.42°, 35.28°, 50.75°, and 60.33° correspond to the (111), (200), (220), and (311) crystal planes of $Mn_xZr_{1-x}O_2$ solid solution (JCPDS PDF#77-2157), respectively (Figure 1a). On the contrary, the low Mn/Zr ratio resulted in the mixture phase formation, such as ZrO_2 (JCPDS PDF# 78-0048), or a small amount of solid solution, which is ascribed to the difference in ion radius. The ion radius of Mn^{n+} cations (Mn^{2+}(0.83 Å), Mn^{3+}(0.64 Å) and Mn^{4+}(0.53 Å)) is smaller than Zr^{4+}(0.84 Å). Therefore, it can be speculated that Mn cations readily partially replace Zr cations in the host lattice, whereas it is very difficult [24]. Additionally, the incorporation of Mn dramatically changes the crystal phase of zirconia (Figure 1b). Moreover, the preparation route played an important role in regulating the intensity of characteristic peaks of the $Mn_xZr_{1-x}O_2$ solid solution. The two-step precipitation strategy is easier to obtain a high content of active phase solid solution as well as trace amounts of manganese oxide. Besides, it can be found that TP-Mn2Zr3 has more obvious (111) crystal plane characteristic peaks compared to CP-Mn2Zr3.; the content of (111) crystal plane of TP-Mn2Zr3 sample accounted for 51.4%, which is considered the active center [31], while the CP-Mn2Zr3 is ca. 49.3%. This is the reason why the TP-Mn2Zr3 sample has a better catalytic performance. The sample (MP-Mn2Zr3) prepared by mechanical ball mills was as a reference. The result showed that the separated mixture of ZrO_2 and Mn_2O_3 oxides caused no synergistic effect between MnO_x and ZrO_2, and a poor catalytic activity for toluene oxidation under the ball milling conditions.

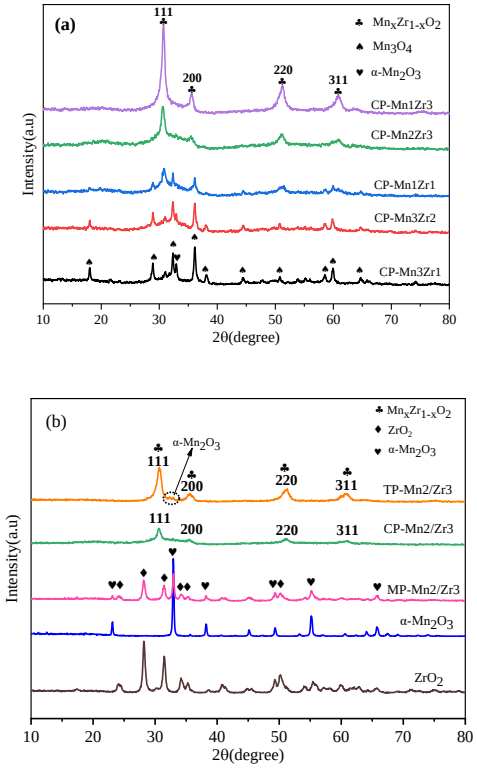

Figure 1. XRD patterns of catalysts with different molar ratios of Mn/Zr (**a**) and different preparation routes (**b**) (two-step precipitation (TP); conventional coprecipitation (CP); ball milling process (MP)).

Moreover, the lattice parameters and grain size of CP-Mn2Zr3, TP-Mn2Zr3, MP-Mn2Zr3, ZrO_2, and α-Mn_2O_3 samples were summarized in Table 1. Compared with MP-Mn2Zr3 and CP-Mn2Zr3, the TP-Mn2Zr3 catalyst has the lowest lattice parameters (5.04 Å) and the smallest grain size (8.4 nm). Indeed, Mn cations with different valence exhibit a different ionic radius. The more Mn^{n+} cations (Mn^{2+}, Mn^{3+}, and Mn^{4+}) with smaller radii (0.83, 0.64, and 0.53 Å, respectively) incorporated into c-zirconia to replace the Zr^{4+} (0.84 Å) can reduce the lattice parameters [28,35,36]. Based on this, we can infer that

the improved preparation process is more beneficial to the synthesis of the $Mn_xZr_{1-X}O_2$ solid solution and decreases the grain size.

Table 1. Data obtained from XRD analyses of two-step precipitation (TP), conventional coprecipitation (CP), ball milling process (MP)-Mn2Zr3, ZrO_2, and α-Mn_2O_3 samples.

Samples	*a* (Å)	*b* (Å)	*c* (Å)	*v* (Å^3)	Grain Size (nm) [a]
TP-Mn2Zr3	5.04	-	-	128	8.4
CP-Mn2Zr3	5.05	-	-	128.8	11.3
MP-Mn2Zr3	-	-	-	-	21.5
ZrO_2	5.87	4.86	5.20	148.3	16.6
α-Mn_2O_3	9.42	9.42	9.42	835.9	32.2

[a] The average crystal size was calculated by the Scherrer equation from the XRD data.

2.1.2. BET Analysis

It was accepted that the catalytic activity of nanocatalysts is closely related to their surface texture, such as specific surface area, average pore size, and pore volume. Figure 2 shows the nitrogen adsorption-desorption curves of as-obtained catalysts (TP-Mn2Zr3, CP-Mn2Zr3, and MP-Mn2Zr3), and it can be observed that these catalysts have similar adsorption isotherms, which can be classified as typical type IV adsorption isotherms based on the IUPAC classification [37]. Hysteresis loops demonstrated relative pressure in the range of 0.4–1 in all three samples, and there was no adsorption saturation platform in the range of higher relative pressure, suggesting the catalysts have an irregular pore structure that may be caused by the slit-shaped pores. The type IV isotherm is usually the basis for judging whether there are mesopores in the catalyst materials [8,38]. Considering the presence of type IV adsorption isotherm and H3 hysteresis loop in the catalyst, it can be determined that irregular mesopores were formed in all the catalysts [39]. Figure 2b shows the pore size distribution of the catalyst, which further confirmed the existence of the mesoporous structure in the catalysts. The pore size mainly distributed in the range of 2–40 nm and centered around 10 nm. Specifically, the value of the specific surface area, average pore diameter, and pore volume of the catalyst were listed in Table 2. It was observed that the catalyst prepared by mechanical stirring showed the lowest specific surface area, only 23.7 m^2/g, whereas the catalyst doped with Zr obviously demonstrated an improved specific surface area. The specific surface areas of TP-Mn2Zr3 and CP-Mn2Zr3 catalysts were 99.7 and 139.5 m^2/g, respectively, which may promote the exposure of active sites on the surface of the catalysts [31] and contribute to the improved catalytic performance. Among these oxides, the average pore sizes of TP-Mn2Zr3, CP-Mn2Zr3, and MP-Mn2Zr3 catalysts are 10.8, 5.9, and 13.5 nm, respectively. It was found that the TP-Mn2Zr3 catalyst has the largest pore volume of 0.27 cm^3/g, followed by CP-Mn2Zr3 (0.20 cm^3/g) and MP-Mn2Zr3 (0.08 cm^3/g) catalysts.

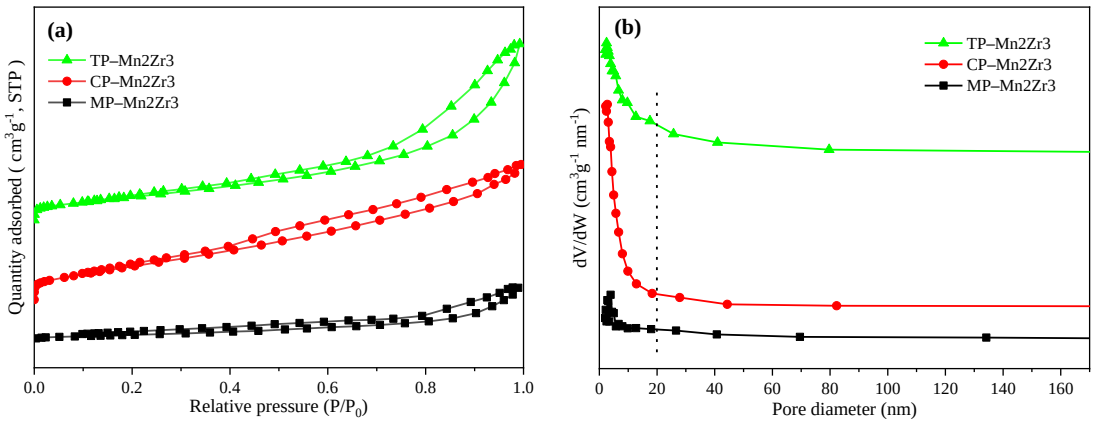

Figure 2. Nitrogen adsorption-desorption isotherms (**a**) and BJH pore-size distributions (**b**) of TP-Mn2Zr3, CP-Mn2Zr3, and MP-Mn2Zr3 catalysts.

Table 2. The surface area, average pore diameter, and pore volume of TP-Mn2Zr3, CP-Mn2Zr3, and MP-Mn2Zr3 catalysts.

Samples	S_{BET} (m^2/g)	Average Pore Diameter (nm) [a]	Pore Volume (cm^3/g) [b]
TP-Mn/Zr = 2/3	99.7	10.8	0.27
CP-Mn/Zr = 2/3	139.5	5.9	0.20
MP-Mn/Zr = 2/3	23.7	13.5	0.08

[a] Bases on the total adsorption average pore width (4V/A by BET, A = S_{BET}). [b] Based on the BJH Adsorption cumulative volume.

2.1.3. HRTEM Analysis

In order to further study the morphology of the catalysts, TEM experiments were carried out on the CP-Mn2Zr3 and TP-Mn2Zr3 catalysts, as shown in Figure 3. The results suggested that both CP-Mn2Zr3 and TP-Mn2Zr3 exhibit morphology of nanoparticles (Figure 3a,c) and the lattice spacings of ca. 2.54 and 2.94 Å, well attributed to the (111) crystal plane and (200) crystal plane of the $Mn_xZr_{1-x}O_2$ solid solution, respectively (Figure 3b,d). This is in line with the XRD results. Therefore, it can be inferred that Mn ions are readily embedded in the lattice of ZrO_2 and form Mn-Zr solid solution via co-precipitation or optimized two-step precipitation route and lead to the phase transformation from monoclinic zirconium dioxide into cubic zirconium dioxide [26].

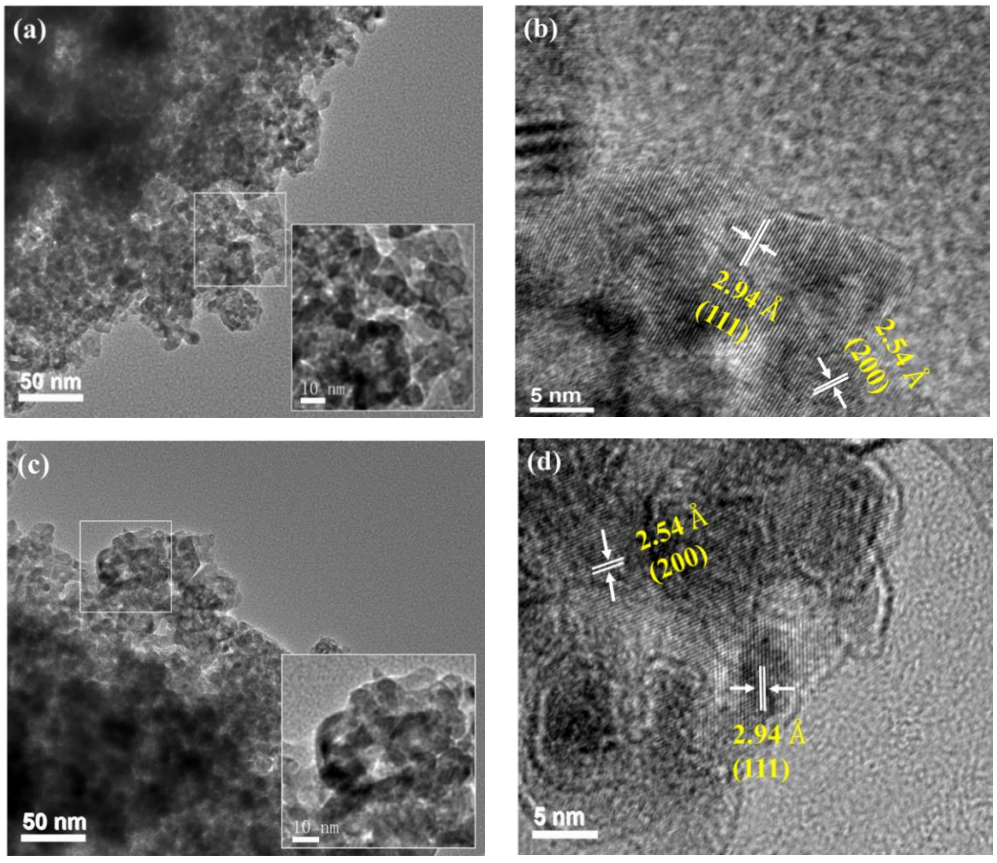

Figure 3. High resolution transmission electron microscope (HRTEM) images of CP-Mn2Zr3 (**a**,**b**) and TP-Mn2Zr3 (**c**,**d**).

2.1.4. XPS Analysis

XPS experiments were performed to analyze the components and valence states of elements, as shown in Figure 4 and Table 3. It was observed that the surface elements of the catalyst are mainly composed of O (ca. 530 eV), Zr (ca. 183 eV), and Mn (ca. 642 eV) (Figure 4a) [30,40]. Figure 4b shows the XPS spectra of Mn 2p; it was integrated into

two characteristic peaks by deconvolution. The characteristic peaks located at 641.7 eV and 643.4 eV can be attributed to Mn^{3+} and Mn^{4+} species, respectively [1,17,41].

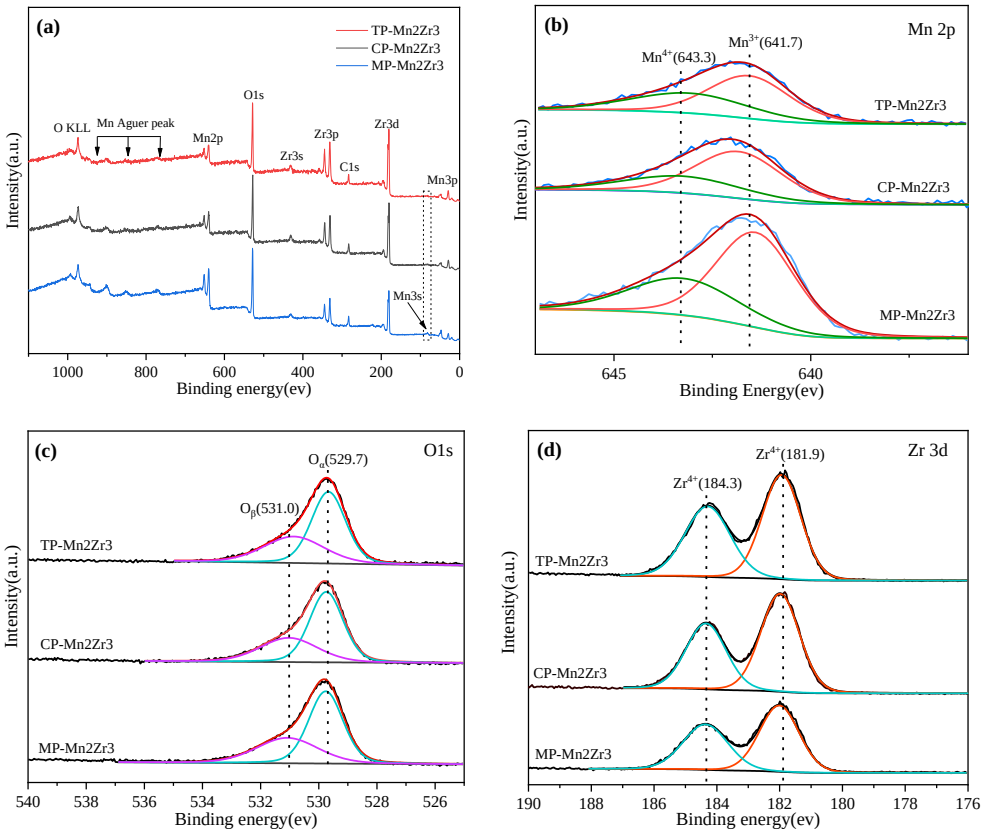

Figure 4. XPS spectra of (**a**) full spectra, (**b**) Mn 2p, (**c**) O 1s, (**d**) Zr 3d over TP, CP, and MP-Mn2Zr3.

Table 3. Analysis of the surface composition and content of samples based on XPS results.

Samples	Surface Element (at%)			Bind Energy				Surface Element Molar Ratio	
	Mn 2p	Zr 3d	O 1s	Mn^{4+}	Mn^{3+}	O_α	O_β	Mn^{4+}/Mn^{3+}	O_β/O_α
TP-Mn2Zr3	15.92	18.63	65.46	643.3	641.7	529.7	531.0	0.68	0.65
CP-Mn2Zr3	17.37	17.69	64.94	643.5	641.9	529.7	531.0	0.50	0.59
MP-Mn2Zr3	29.70	11.04	59.25	643.4	641.5	529.7	531.1	0.53	0.63

Furthermore, the ratio of Mn^{4+}/Mn^{3+} of the catalyst calculated based on the relative area was closely related to the preparation routes. The TP-Mn2Zr3 catalyst prepared by an improved precipitation method had a higher Mn^{4+}/Mn^{3+} value, which reached 0.68, which followed the MP-Mn2Zr3 (0.53) and CP-Mn2Zr3 catalysts (0.50), respectively. The strong interaction between Mn and Zr in Mn-Zr solid solution can promote the occurrence of the charge transfer process and produce more Mn^{4+} [30], which plays a key role in the catalytic degradation of toluene. In other words, the stronger interaction between Mn and Zr in the catalyst of TP-Mn2Zr3 can be conducive to higher catalytic oxidation of toluene. Meanwhile, it is widely accepted that the oxygen mobility of manganese-based oxides is closely related to the transformation ability of manganese species between different valence states, and the increase of the concentration of high valence metal cations promotes the chemical potential and mobility of oxygen [42].

O 1s XPS spectra of the three catalysts were exhibited in Figure 4c, which can be split into two peaks by deconvolution, the bind-energy located at 529.0−530.0 eV and 531.0−532.0 eV can be ascribed to the surface lattice oxygen (O_α) and chemisorbed oxygen and/or defect oxides (O^{2-}, O_2^{2-}, or O^-) (O_β) [28], respectively. It was noted that the content of O_α is more than 60% for the three samples, suggesting the O_α is dominated. Furthermore, the decreasing trend of

O_β/O_α value is as follows: TP-Mn2Zr3(0.65) > MP-Mn2Zr3(0.63) > CP-Mn2Zr3 (0.59), which is positively correlated with the value of Mn^{4+}/Mn^{3+}(TP-Mn2Zr3 (0.68) > MP-Mn2Zr3(0.53) > CP-Mn2Zr3 (0.50)). It was reported that both lattice oxygen and chemisorbed oxygen and/or defect oxides are active oxygen species that can participate in the oxidation of toluene, which improves the oxidation performance of the catalyst [19,35]. Herein, the optimized coprecipitation catalyst displays better catalytic activity due to the contribution of lattice oxygen and absorbed oxygen.

The spin-splitting peaks of the Zr 3d orbit can be observed in Figure 4d, centered at 181.9 eV and 184.3 eV and belong to $3d_{5/2}$ and $3d_{3/2}$ orbit, respectively, suggested that Zr cations exist in the catalyst in the form of tetravalent [30]. Meanwhile, it was found that there was hardly a change in the position of the Zr 3D orbital splitting peak in TP-Mn2Zr3, CP-Mn2Zr3, and MP-Mn2Zr3 samples. It was worth noting that the XPS signal peak of Zr in TP-Mn2Zr3 and CP-Mn2Zr3 samples originated from the Mn-Zr solid solution, while the signal peak of Zr in the MP-Mn2Zr3 sample was derived from pure zirconia. This indicates that the Zr^{4+} ion is very stable [43], though the Mn^{n+} ions were entered the framework of ZrO_2. Moreover, the proportion of Mn, Zr, and O in the catalyst is related to the preparation routes (Table 3). The order of the proportion of Mn elements follows: MP-Mn2Zr3 > CP-Mn2Zr3 > TP-Mn2Zr3, while that of Zr and O is the opposite; this suggested that the concentration of Mn-Zr solid solution various with the content of Mn ions entered the framework of ZrO_2.

2.1.5. H_2-TPR Results Analysis

The H_2-TPR experiments were employed to investigate the reducibility of the catalysts. The H_2-TPR cures of TP-Mn2Zr3, CP-Mn2Zr3, and MP-Mn2Zr3 samples in the range of 100–700 °C are shown in Figure 5. There exist three obvious characteristic peaks of hydrogen consumption. It was reported that about 15 wt.% of MnO is soluble in ZrO_2 due to the solidified eutectic temperature [44]. Herein, the three characteristic peaks of catalysts were mainly attributed to the reduction of MnO_x, in which Peak 1 located below 250 °C shows the reduction of amorphous MnO_x, dispersed on the surface of Mn-Zr solid solution, and peak 2 (250–380 °C) should be linked to the reduction of Mn_2O_3 to Mn_3O_4, while peak 3 (380–480 °C) corresponds to the reduction of Mn_3O_4 to MnO, respectively [26,31,45]. Moreover, the TP-Mn2Zr3 and CP-Mn2Zr3 catalysts behave an excellent low-temperature reduction performance compared to that of MP-Mn2Zr3. Especially for the TP-Mn2Zr3 sample, the locations of reduction peaks are separately reduced to 224, 303, and 400 °C, suggesting it possessed a stronger mobility of reactive oxygen species and leads to a better catalytic activity for VOCs abatement [31].

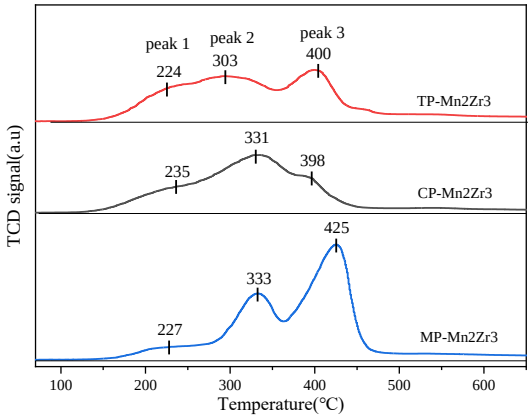

Figure 5. H_2-TPR profiles of TP-Mn2Zr3, CP-Mn2Zr3, and MP-Mn2Zr3 catalysts.

It was found that the reduction temperature of pure zirconia usually appears above 600 °C, and the incorporation of Mn into the framework of zirconia to form a solid solution of $Mn_xZr_{1-x}O_2$ would contribute to the decreasing of reduction temperature [26,29]. In

this contribution, the reduction peak of zirconia was not observed on the MP-Mn2Zr3 catalyst, indicating that $Mn_xZr_{1-x}O_2$ species cannot be formed by the ball milling process. In contrast, the shouldered temperature reduction peak (ca. 400 °C) was displayed in both TP-Mn2Zr3 and CP-Mn2Zr3 catalysts, which may be the result of the synergistic interaction between the surface MnO_x and ZrO_2 alloyed to form Mn-Zr solid solution [31,46], which well corresponds to the XRD results.

2.2. Evaluation of Catalytic Activity

The catalytic oxidation performance of the synthesized catalysts for toluene abatement was assessed. The functional cures between the conversion of toluene on the catalysts and reaction temperature are depicted in Figure 6. All the catalysts can achieve complete catalytic oxidation for toluene below 300 °C. As shown in Figure 6a, the CP-Mn2Zr3 catalyst exhibits better catalytic oxidation activity for toluene. The values of T_{50} (the 50% conversion of 1000 ppm toluene) and T_{90} (the 90% conversion of 1000 ppm toluene) of the CP-Mn2Zr3 catalyst are 270 °C and 278 °C, respectively. In addition, the order of catalytic ability of catalysts is depicted as CP-Mn2Zr3 > CP-Mn3Zr1 > CP-Mn3Zr2 > CP-Mn1Zr1 > CP-Mn1Zr3. It is evident that the catalytic activity was closely linked with the Mn/Zr ratio, which controlled the component of the Mn-Zr solid solution. Thereby, it can be inferred that the Mn-Zr solid solution is in the active phase and greatly influences the catalytic activity for toluene.

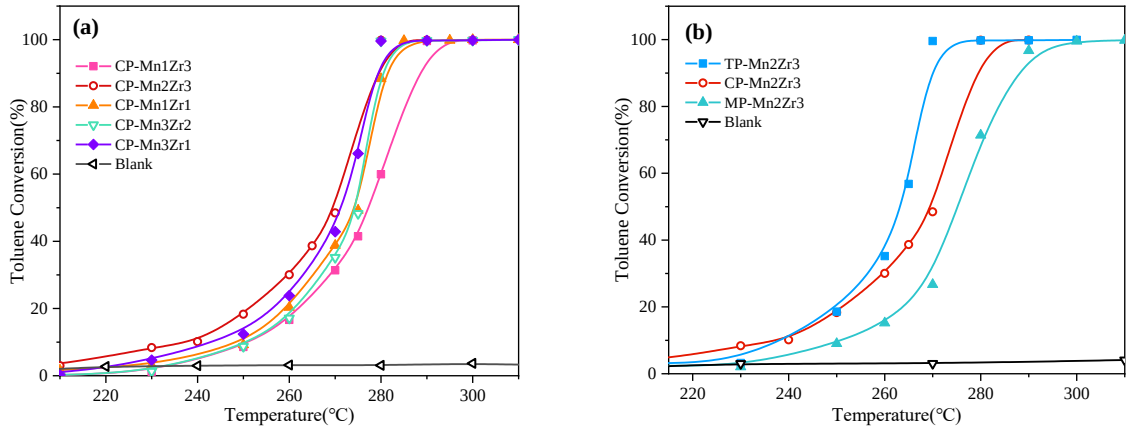

Figure 6. Activity test of catalysts with different molar ratios of Mn/Zr (**a**) and prepared by different strategies (**b**).

Moreover, the catalytic activity assessing experiments were also carried out on CP-Mn2Zr3, TP-Mn2Zr3, and MP-Mn2Zr3 catalysts, and the results are depicted in Figure 6b. Obviously, the TP-Mn2Zr3 catalyst exhibits a better catalytic performance with T_{50} and T_{90} values of 263 °C and 269 °C, respectively, followed by CP-Mn2Zr3. The performance of the catalyst with MP-Mn2Zr3 is the lowest, with T_{50} and T_{90} values of 275 °C and 287 °C, which is much lower than the TP-Mn2Zr3 and CP-Mn2Zr3 catalysts. The results clearly show that the TP-Mn2Zr3 and CP-Mn2Zr3 catalysts with the existence of the Mn-Zr solid solution exhibit higher catalytic activity for toluene abatement than that of the MP-Mn2Zr3 catalyst without the formation of the Mn-Zr solution. The outstanding catalytic performance of the TP-Mn2Zr3 catalyst for toluene should be attributed to the more exposed defect (111) crystal plane of $Mn_xZr_{1-x}O_2$ and the improved capacity of mobility of active oxygen.

The stability of the texture for the Mn-Zr catalysts will determine their potential application to some extent. In this work, five consecutive catalytic light-off cycle tests were performed on the TP-Mn2Zr3 and CP-Mn2Zr3 catalysts, and the results are shown in Figure 7. The value of the T_{90} value of the cycle 2 experiment for the TP-Mn2Zr3 catalyst is 259 °C, which is lower than that of the cycle 1 experiment (269 °C), and runs 3, 4, and 5 on the TP-Mn2Zr3 catalyst maintain a similar value of T_{90} (259 °C ± 1). On the contrary, the CP-Mn2Zr3 catalyst performed inferior cyclic stability, in which the value of T_{90} for cycles 1, 2, 3, 4, and 5 was 278, 269, 264, 264, and 269 °C, respectively. The enhanced

oxidation performance for both catalysts after running the first experiment should be attributed to the activation effect at 300 °C [8]. To view the cyclic stability directly, the function curves between cycle times and toluene conversion at 265 °C are depicted as the inset of Figure 7a,b, which imply that the TP-Mn2Zr3 catalyst exhibited better cycle stability. Conversely, the order of cyclic stability of CP-Mn2Zr3 obeys the volcanic model, which implies the inferior stability of CP-Mn2Zr3.

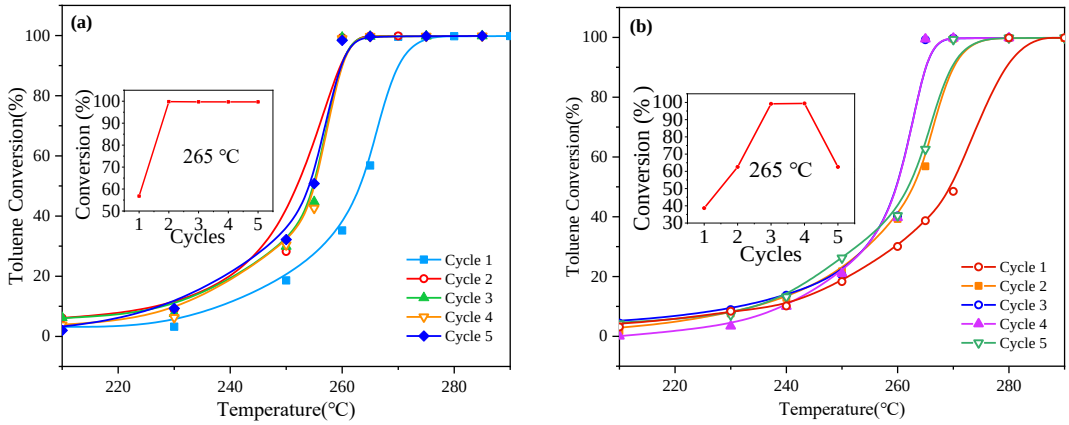

Figure 7. Activity cycle test of the TP-Mn2Zr3 catalyst (**a**) and the CP-Mn2Zr3 catalyst (**b**).

Based on studies reports, the bimetal oxide catalysts involve two reaction mechanisms in the oxidation for toluene, namely the Langmuir–Hinshelwood (L-H) and Mars–van Krevelen (Mv-K) mechanisms. Increasing the temperature, the L-H mechanism is gradually weakened, and the Mv-K mechanism gradually occupies a dominant position. The adsorbed oxygen directly oxidizes the adsorbed organic molecules, which is accorded to the L-H mechanism; on the other hand, lattice oxygen is activated at a higher temperature, and the consumed lattice oxygen can be readily supplemented from gaseous oxygen, which obeys the Mv-K mechanism [42,47].

Figure 8a reveals the effect of different WHSVs on the activity of the TP-Mn2Zr3 catalyst. Obviously, the value of T_{90} is positively correlated with WHSV; in other words, a longer contact time is beneficial to improve the catalytic performance. The longevity experiments for 3000 min were performed on TP-Mn2Zr3 and CP-Mn2Zr3 catalysts, as shown in Figure 8b. It was worth noting that the TP-Mn2Zr3 catalysts maintained a splendid catalytic activity (>90% toluene conversion). While the CP-Mn2Zr3 catalyst declined a lot after 1000 min and the value of toluene degradation was sharply decreased to about 50%, the conversion of toluene was only kept at ca. 33% after the 3000 min combustion reaction.

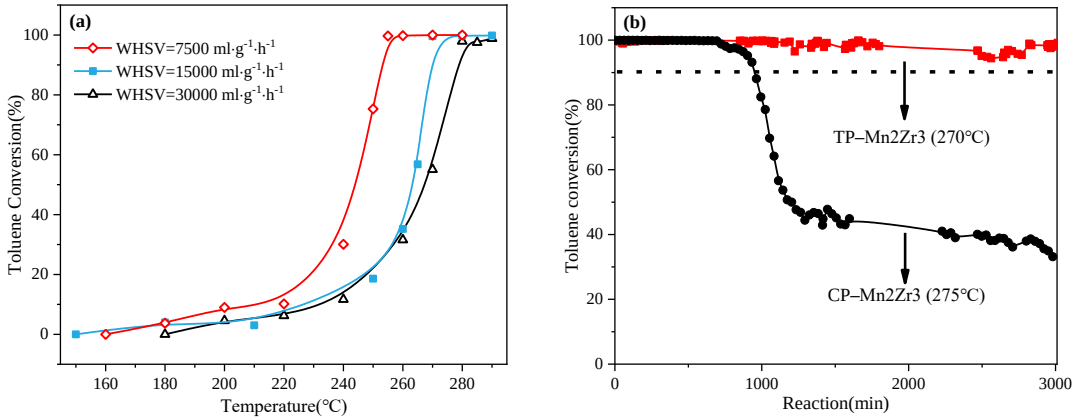

Figure 8. The effect of different WHSVs on the activity of the TP-Mn2Zr3 catalyst (**a**); Longevity test over TP-Mn2Zr3 and CP-Mn2Zr3 in 1000 ppm toluene (**b**).

3. Discussion

It was widely accepted that the physical and chemical properties, such as component of active phase, specific surface area, Mn valence, concentration of adsorbed oxygen/lattice oxygen and reduction ability, can command the activity of the catalyst [48]. For the component factor of the active phase, we found that the ratio of Mn/Zr and their synthesis routes play a vital role in adjusting the content of active centers, and a low molar ratio (<2/3) of Mn/Zr would lead to the formation of a solid solution of $Mn_xZr_{1-x}O_2$. As the molar ratio goes up, a second phase, such as Mn_2O_3 and Mn_3O_4, will be formed, as depicted in Figure 1a. This is mainly attributed to the solubility limit of manganese in the zirconia lattice [44]. However, a more complex mixed components does not necessarily result in a better catalytic activity, as the CP-Mn2Zr3 catalyst presented a better catalytic performance among the samples prepared by the co-precipitation process (Figure 6a). Moreover, the improved co-precipitation route can further promote the exposure of the active centers and enhance the catalytic performance. Therefore, it can be inferred that the optimized catalytic activity is linked to components of the active phase and mainly hinges on the ratio of Mn/Zr and their synthesis routes. On the other hand, co-precipitation and improved co-precipitation routes are ready to prepare catalysts with a large specific surface area and enhance their catalytic activities.

In addition, the concentrations of Mn^{4+} and O_α species of oxidizing catalyst were crucial for the oxidative degradation of VOCs [43,49]. The order of the O_β /O_α follows in descending order as Mn^{4+}/Mn^{3+}, which was depicted as TP-Mn2Zr3 > MP-Mn2Zr3 > CP-Mn2Zr3, indicating the concentration of Mn^{4+} was positively correlated with the content of oxygen vacancy [40]. In combination with the results of catalytic activity and components of active phase, the improved catalytic activity should be attributed to the promoted effects of the solid solution of $Mn_xZr_{1-x}O_2$. Moreover, the shouldered shape of the reduction peak for TP-Mn2Zr3 and CP-Mn2Zr3 catalysts can also account for the formation of $Mn_xZr_{1-x}O_2$ active species, which corresponds well with the results of XRD.

It was reported that the catalytic mechanism of toluene on Mn-based catalysts involves the Mv-K and L-H mechanism. Both lattice oxygen and adsorbed oxygen species can participate in the activation-oxidation process of VOCs [42,47,50]. In this paper, the enhanced catalytic activity of Mn-Zr catalysts may be ascribed to the collective effects of manganese zirconium bimetal because the formation of the solid solution of $Mn_xZr_{1-x}O_2$ would be conducive to decrease the formation energy of oxygen vacancy; the oxygen molecule was absorbed and activated to active oxygen to enhance catalytic activity. Furthermore, the oxygen molecule is easily adsorbed on the defective (111) surface of the Mn-Zr catalyst with oxygen vacancy, and the distance of O–O bond was elongated, which probably suggested that the absorbed O_2 is easily activated and broken, which is in favor of the quick replenishment of consumed oxygen molecular during VOCs combustion [31]. This is in good agreement with the H_2-TPR results. Therefore, it is supposed that the enriched exposure of the defective (111) surface of the $Mn_xZr_{1-x}O_2$ active species would lead to better catalytic activity for toluene combustion, and this can account for the outstanding performance of TP-Mn2Zr3.

4. Materials and Methods

4.1. Materials

Zirconium (IV) oxynitrate hydrate ($ZrO(NO_3)_2{\cdot}H_2O$) and Manganese nitrate ($Mn(NO_3)_2$) solution 50 wt.% were purchased from Chengdu Hua Xia Chemical Reagent Co., Ltd. (Chengdu, China). Ammonia ($NH_3{\cdot}H_2O$) (25~28%) reagent was purchased from Chengdu Ke Long chemicals Co., Ltd (Chengdu, China). All the reagents are an analytical reagent (AR), with no need for further treatment.

4.2. Catalyst Preparation

Firstly, Mn-Zr hybrids catalysts with different ratios were prepared by conventional optimized co-precipitation routes [24,25]. In a typical preparation, manganese nitrate

solution (50 wt.%) (3.58, 7.16, 7.16, 10.74, and 10.74 g, respectively) and zirconium (IV) oxynitrate hydrate (7.48, 7.48, 4.99, 4.99, and 2.49 g, respectively) were added into 100 mL deionized water and vigorously stirred for 2 h to form homogeneous solution, respectively. Then ammonia was added dropwise until PH = 9 (Scheme 1a). The obtained precipitates are filtrated and washed until pH = 7. After that, the precipitate was dried in an oven at 90 °C for 5 h, followed by calcination at 550 °C for 5 h under an air atmosphere. Herein the ratios of Mn/Zr were listed as 1/3, 2/3, 1/1, 3/2, and 3/1, marked as CP = Mn1Zr3, CP = Mn2Zr3, CP = Mn1Zr1, CP = Mn3Zr2, and CP = Mn3Zr1, respectively.

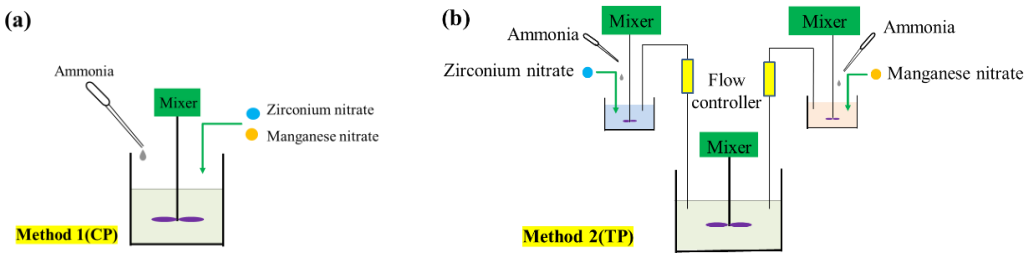

Scheme 1. The synthesis of catalyst by coprecipitation (**a**), and optimized coprecipitation (**b**).

The TP-Mn2Zr3 catalysts were prepared by two-step precipitation strategies. Specifically, manganese nitrate solution (50 wt.%) (7.16 g) and zirconium (IV) oxynitrate hydrate (7.48 g) were added into 50 mL deionized water and vigorously stirred for 2 h to form a homogeneous solution, respectively. Then ammonia was added dropwise into the two solutions until pH = 9 (Scheme 1b). We mixed the two solutions under vigorous stirring for 2 h. The washing, filtering, drying and calcining processes were the same procedures for CP-Mn2Zr3. Additionally, the final product is recorded as TP-Mn2Zr3. For comparison, MnO_x and ZrO_2 catalysts were prepared by the above routes. Besides, the MP-Mn2Zr3 sample was prepared by mechanical ball mill of a mixture of MnO_x and ZrO_2. The ball milling experiment was carried out on a planetary ball mill (XQM-0.4). Actually, the stainless-steel balls with different diameters (15, 12, 10, 8, and 5 mm) were mixed and added into a ball milling tank (50 mL) and then stirred for 2 h at 400 r/min. In addition, the total mass of stainless-steel balls was 150 g, and the mass of Mn_2O_3 and ZrO_2 was 1.84 g and 2.16 g, respectively, to keep the molar ratio of Mn/Zr at 2/3.

4.3. Catalyst Activity Evaluation

The catalytic degradation of toluene was assessed in a fixed-bed stainless reactor (id = 7 mm). Prior to the activity test, the catalyst (0.20 g, 40–60 mesh) and quartz sands (0.30 g, 40–60 mesh) were well mixed and then loaded into the center of the reactor and activated at 300 °C for 1 h with a 60 mL/min air flow rate. After that, the temperature was dropped to 150 °C, and 1000 ppm toluene gas was continuously fed into the fixed-bed reactor; the total flow is controlled at 50 mL/min to correspond to a weight hourly space velocity (WHSV) of 15,000 mL g_{cat}^{-1} h^{-1}. In addition, the catalytic activity of TP-Mn2Zr3 was tested under different WHSVs. The exhausted gas from a fixed-bed reactor was analyzed using a gas chromatography device (SP-7890 PLUS, Rui Hong Co, Ltd., Tengzhou, China) with a flame ionization detector (FID) and equipped polyethylene glycol capillary column and a thermal conductivity detector (TCD). The activity of the catalyst was measured by the toluene conversion (X_{con}), which can be calculated as follow:

$$X_{con} = \frac{C_{in} - C_{out}}{C_{in}} \quad (1)$$

where C_{in} stand for the inlet toluene concentration, and C_{out} represent the outlet toluene concentration after 30 min reaction.

4.4. Catalyst Characterization

The investigation of the phase composition of the catalysts was carried out by the Rigaku DX-2700 (Rigaku, Tokyo, Japan) diffractometer equipment with Cu-Kα (λ = 0.154 nm) as the radiation source. The scan started from 10 to 80° with a scanning rate of 0.06°/s. The results of the specific surface area and pore size distribution of the catalysts were obtained by nitrogen adsorption and desorption experiments on V-SorbX800 (Jin Aipu, Beijing, China) equipment at −196 °C. The microstructure of the fresh catalysts was investigated by an FEI Tecnai G2 F20 (GCEMarket, Blackwood, NJ, America) Transmission electron microscopy (TEM) equipped with a HAADF detector. The TEM experiment was carried out in an accelerated voltage environment of 2000 volts. The X-ray photoelectron spectroscopy was obtained by the PHI 5000 (Ulvac-PHI, Inc., Kanagawa, Japan) spectrometer with Al Kα as the radiation. The obtained binding energy was calibrated with C1s (284.8 eV) as the internal reference standard. AutoChem2920 (Micromeritics Instrument Corp, Norcross, GA, USA) chemisorption analyzer was used to analyze the reduction performance of the fresh catalysts. Before the reduction process, 30 mg prepared catalyst was pretreated at 300 °C for 1 h in an N_2 atmosphere (30 mL/min) to remove oxygen.

5. Conclusions

In this paper, a series of Mn-Zr catalysts with different Mn/Zr ratios were successfully prepared via co-precipitation and improved co-precipitation routes, and their catalytic performance for toluene combustion was evaluated. It was found that the TP-Mn2Zr3 catalyst possesses the lowest T_{50} and T_{90} temperature at 263 and 269 °C and exhibits practical cycle stability. Moreover, the relationship between the catalyst performance and texture was deeply investigated via some characterization techniques, including XRD, HRTEM, BET, H_2-TPR, and XPS. The results showed that the doping of Mn enables the crystal structure of ZrO_2 to transform from the monoclinic to the cubic phase, exposes the stable c-ZrO_2 (111) phase, and increases the specific surface area of Mn-Zr bimetal catalysts via the co-precipitation strategy. In particular, the optimized co-precipitation process enriches more exposure of the defective (111) surface of the $Mn_xZr_{1-x}O_2$ solid solution to active oxygen molecular and more oxygen vacancy as well as the higher concentration of Mn^{4+}, which is conducive to the mobility of oxygen to improve their catalytic activity for toluene combustion. This new observation will provide a promising strategy to design excellent catalysts for VOCs abatement.

Author Contributions: X.H.: completing the experiments and writing—original manuscript. L.L. (Luming Li): project administration, providing the experiment ideas, and writing—review. R.L., H.L., L.L. (Li Lan) and W.Z.: analysis and agree to take responsibility for the accuracy and authenticity of the research work. All authors have read and agreed to the published version of the manuscript.

Funding: This research was supported by the Open Fund of the Key Laboratory of Coarse Cereal Processing, Ministry of Agriculture and Rural Affairs, Sichuan Engineering and Technology Research Center of Coarse Cereal Industrialization (2020CC020).

Data Availability Statement: The data of this research is available within the manuscript.

Acknowledgments: We are grateful to the experimental platform provided by the Institute of Environmental Catalysis and Dust Treatment of Chengdu University. Thanks to the TEM characterization provided from Xiamen University and the XPS analyzed provided by Institute for Advanced Study of Chengdu University.

Conflicts of Interest: The authors declare no conflict of interest.

References

1. Liu, Y.; Dai, H.; Du, Y.; Deng, J.; Zhang, L.; Zhao, Z.; Au, C.T. Controlled preparation and high catalytic performance of three-dimensionally ordered macroporous $LaMnO_3$ with nanovoid skeletons for the combustion of toluene. *J. Catal.* **2012**, *287*, 149–160. [CrossRef]
2. Li, W.B.; Wang, J.X.; Gong, H. Catalytic combustion of VOCs on non-noble metal catalysts. *Catal. Today* **2009**, *148*, 81–87. [CrossRef]

3. Saqer, S.M.; Kondarides, D.I.; Verykios, X.E. Catalytic Activity of Supported Platinum and Metal Oxide Catalysts for Toluene Oxidation. *Top. Catal.* **2009**, *52*, 517–527. [CrossRef]
4. Mustafa, M.F.; Fu, X.; Liu, Y.; Abbas, Y.; Wang, H.; Lu, W. Volatile organic compounds (VOCs) removal in non-thermal plasma double dielectric barrier discharge reactor. *J. Hazard. Mater.* **2018**, *347*, 317–324. [CrossRef]
5. He, C.; Cheng, J.; Zhang, X.; Douthwaite, M.; Pattisson, S.; Hao, Z. Recent Advances in the Catalytic Oxidation of Volatile Organic Compounds: A Review Based on Pollutant Sorts and Sources. *Chem. Rev.* **2019**, *119*, 4471–4568. [CrossRef]
6. Ma, X.Y.; Yu, X.L.; Yang, X.Q.; Lin, M.Y.; Ge, M.F. Hydrothermal Synthesis of a Novel Double-Sided Nanobrush Co_3O_4 Catalyst and Its Catalytic Performance for Benzene Oxidation. *ChemCatChem* **2019**, *11*, 1214–1221. [CrossRef]
7. Yang, X.; Yu, X.; Lin, M.; Ge, M.; Zhao, Y.; Wang, F. Interface effect of mixed phase Pt/ZrO_2 catalysts for HCHO oxidation at ambient temperature. *J. Mater. Chem. A* **2017**, *5*, 13799–13806. [CrossRef]
8. Li, L.; Chu, W.; Liu, Y. Insights into key parameters of MnO_2 catalyst toward high catalytic combustion performance. *J. Mater. Sci.* **2021**, *56*, 6361–6373. [CrossRef]
9. Xie, S.; Deng, J.; Liu, Y.; Zhang, Z.; Yang, H.; Jiang, Y.; Arandiyan, H.; Dai, H.; Au, C.T. Excellent catalytic performance, thermal stability, and water resistance of 3DOM Mn_2O_3-supported Au–Pd alloy nanoparticles for the complete oxidation of toluene. *Appl. Catal. A Gen.* **2015**, *507*, 82–90. [CrossRef]
10. Yao, X.; Yu, Q.; Ji, Z.; Lv, Y.; Cao, Y.; Tang, C.; Gao, F.; Dong, L.; Chen, Y. A comparative study of different doped metal cations on the reduction, adsorption and activity of $CuO/Ce_{0.67}M_{0.33}O_2$ ($M = Zr^{4+}$, Sn^{4+}, Ti^{4+}) catalysts for NO+CO reaction. *Appl. Catal. B Environ.* **2013**, *130–131*, 293–304. [CrossRef]
11. Chung, W.-C.; Mei, D.-H.; Tu, X.; Chang, M.-B. Removal of VOCs from gas streams via plasma and catalysis. *Catal. Rev.* **2018**, *61*, 270–331. [CrossRef]
12. Sihaib, Z.; Puleo, F.; Garcia-Vargas, J.M.; Retailleau, L.; Descorme, C.; Liotta, L.F.; Valverde, J.L.; Gil, S.; Giroir-Fendler, A. Manganese oxide-based catalysts for toluene oxidation. *Appl. Catal. B Environ.* **2017**, *209*, 689–700. [CrossRef]
13. Craciun, R.; Nentwick, B.; Hadjiivanov, K.; Knözinger, H. Structure and redox properties of MnO_x/Yttrium-stabilized zirconia (YSZ) catalyst and its used in CO and CH4 oxidation. *Appl. Catal. A Gen.* **2003**, *243*, 67–79. [CrossRef]
14. Kim, S.C.; Shim, W.G. Catalytic combustion of VOCs over a series of manganese oxide catalysts. *Appl. Catal. B Environ.* **2010**, *98*, 180–185. [CrossRef]
15. Lin, X.; Li, S.; He, H.; Wu, Z.; Wu, J.; Chen, L.; Ye, D.; Fu, M. Evolution of oxygen vacancies in MnO_x-CeO_2 mixed oxides for soot oxidation. *Appl. Catal. B Environ.* **2018**, *223*, 91–102. [CrossRef]
16. Xie, S.; Liu, Y.; Deng, J.; Zhao, X.; Yang, J.; Zhang, K.; Han, Z.; Dai, H. Three-dimensionally ordered macroporous CeO_2-supported Pd@Co nanoparticles: Highly active catalysts for methane oxidation. *J. Catal.* **2016**, *342*, 17–26. [CrossRef]
17. Afzal, S.; Quan, X.; Zhang, J. High surface area mesoporous nanocast $LaMO_3$ (M = Mn, Fe) perovskites for efficient catalytic ozonation and an insight into probable catalytic mechanism. *Appl. Catal. B Environ.* **2017**, *206*, 692–703. [CrossRef]
18. Zhao, Q.; Fu, L.; Jiang, D.; Ouyang, J.; Hu, Y.; Yang, H.; Xi, Y. Nanoclay-modulated oxygen vacancies of metal oxide. *Commun. Chem.* **2019**, *2*, 11. [CrossRef]
19. Santos, V.P.; Pereira, M.F.R.; Órfão, J.J.M.; Figueiredo, J.L. The role of lattice oxygen on the activity of manganese oxides towards the oxidation of volatile organic compounds. *Appl. Catal. B Environ.* **2010**, *99*, 353–363. [CrossRef]
20. Tang, X.; Li, Y.; Huang, X.; Xu, Y.; Zhu, H.; Wang, J.; Shen, W. MnO_x–CeO_2 mixed oxide catalysts for complete oxidation of formaldehyde: Effect of preparation method and calcination temperature. *Appl. Catal. B Environ.* **2006**, *62*, 265–273. [CrossRef]
21. Tang, W.; Wu, X.; Li, S.; Li, W.; Chen, Y. Porous Mn–Co mixed oxide nanorod as a novel catalyst with enhanced catalytic activity for removal of VOCs. *Catal. Commun.* **2014**, *56*, 134–138. [CrossRef]
22. Morales, M.; Barbero, B.; Cadus, L. Total oxidation of ethanol and propane over Mn-Cu mixed oxide catalysts. *Appl. Catal. B Environ.* **2006**, *67*, 229–236. [CrossRef]
23. Li, H.; Qi, G.; Tana; Zhang, X.; Huang, X.; Li, W.; Shen, W. Low-temperature oxidation of ethanol over a $Mn_{0.6}Ce_{0.4}O_2$ mixed oxide. *Appl. Catal. B Environ.* **2011**, *103*, 54–61. [CrossRef]
24. Gutierrez-Ortiz, J.I.; de Rivas, B.; Lopez-Fonseca, R.; Martin, S.; Gonzalez-Velasco, J.R. Structure of Mn-Zr mixed oxides catalysts and their catalytic performance in the gas-phase oxidation of chlorocarbons. *Chemosphere* **2007**, *68*, 1004–1012. [CrossRef] [PubMed]
25. Fernández López, E.; Sánchez Escribano, V.; Resini, C.; Gallardo-Amores, J.M.; Busca, G. A study of coprecipitated Mn–Zr oxides and their behaviour as oxidation catalysts. *Appl. Catal. B Environ.* **2001**, *29*, 251–261. [CrossRef]
26. Bulavchenko, O.A.; Vinokurov, Z.S.; Afonasenko, T.N.; Tsyrul'nikov, P.G.; Tsybulya, S.V.; Saraev, A.A.; Kaichev, V.V. Reduction of mixed Mn-Zr oxides: In situ XPS and XRD studies. *Dalton Trans.* **2015**, *44*, 15499–15507. [CrossRef]
27. Zhao, Q.; Shih, W.Y.; Chang, H.L.; Shih, W.H. Redox Activity and NO Storage Capacity of MnO_x-ZrO_2 with Enhanced Thermal Stability at Elevated Temperatures. *Ind. Eng. Chem. Res.* **2010**, *49*, 1725–1731. [CrossRef]
28. Zuo, J.; Chen, Z.; Wang, F.; Yu, Y.; Wang, L.; Li, X. Low-Temperature Selective Catalytic Reduction of NO_x with NH_3 over Novel Mn–Zr Mixed Oxide Catalysts. *Ind. Eng. Chem. Res.* **2014**, *53*, 2647–2655. [CrossRef]
29. Choudhary, V.R.; Uphade, B.S.; Pataskar, S.G. Low temperature complete combustion of dilute methane over Mn-doped ZrO_2 catalysts: Factors influencing the reactivity of lattice oxygen and methane combustion activity of the catalyst. *Appl. Catal. A Gen.* **2002**, *227*, 29–41. [CrossRef]

30. Zeng, K.; Li, X.; Wang, C.; Wang, Z.; Guo, P.; Yu, J.; Zhang, C.; Zhao, X.S. Three-dimensionally macroporous $MnZrO_x$ catalysts for propane combustion: Synergistic structure and doping effects on physicochemical and catalytic properties. *J. Colloid Interface Sci.* **2020**, *572*, 281–296. [CrossRef] [PubMed]
31. Yang, X.; Yu, X.; Jing, M.; Song, W.; Liu, J.; Ge, M. Defective $Mn_xZr_{1-x}O_2$ Solid Solution for the Catalytic Oxidation of Toluene: Insights into the Oxygen Vacancy Contribution. *ACS Appl. Mater. Interfaces* **2019**, *11*, 730–739. [CrossRef]
32. Fan, X.; Li, L.; Jing, F.; Li, J.; Chu, W. Effects of preparation methods on $CoAlO_x/CeO_2$ catalysts for methane catalytic combustion. *Fuel* **2018**, *225*, 588–595. [CrossRef]
33. Li, L.; Luo, J.; Liu, Y.; Jing, F.; Su, D.; Chu, W. Self-Propagated Flaming Synthesis of Highly Active Layered CuO-delta-MnO_2 Hybrid Composites for Catalytic Total Oxidation of Toluene Pollutant. *ACS Appl. Mater. Interfaces* **2017**, *9*, 21798–21808. [CrossRef] [PubMed]
34. Lan, L.; Li, H.; Chen, S.; Chen, Y. Preparation of CeO_2–ZrO_2–Al_2O_3 composite with layered structure for improved Pd-only three-way catalyst. *J. Mater. Sci.* **2017**, *52*, 9615–9629. [CrossRef]
35. Hou, Z.; Feng, J.; Lin, T.; Zhang, H.; Zhou, X.; Chen, Y. The performance of manganese-based catalysts with $Ce_{0.65}Zr_{0.35}O_2$ as support for catalytic oxidation of toluene. *Appl. Surf. Sci.* **2018**, *434*, 82–90. [CrossRef]
36. Azalim, S.; Franco, M.; Brahmi, R.; Giraudon, J.M.; Lamonier, J.F. Removal of oxygenated volatile organic compounds by catalytic oxidation over Zr-Ce-Mn catalysts. *J. Hazard. Mater.* **2011**, *188*, 422–427. [CrossRef] [PubMed]
37. Yang, X.Q.; Ma, X.Y.; Yu, X.L.; Ge, M.F. Exploration of strong metal-support interaction in zirconia supported catalysts for toluene oxidation. *Appl. Catal. B Environ.* **2020**, *263*, 118355. [CrossRef]
38. Han, Z.; Yu, Q.; Teng, Z.; Wu, B.; Xue, Z.; Qin, Q. Effects of manganese content and calcination temperature on Mn/Zr-PILM catalyst for low-temperature selective catalytic reduction of NO_x by NH_3 in metallurgical sintering flue gas. *Environ. Sci. Pollut. Res. Int.* **2019**, *26*, 12920–12927. [CrossRef]
39. Huang, N.; Qu, Z.; Dong, C.; Qin, Y.; Duan, X. Superior performance of α@β-MnO_2 for the toluene oxidation: Active interface and oxygen vacancy. *Appl. Catal. A Gen.* **2018**, *560*, 195–205. [CrossRef]
40. Mitran, G.; Chen, S.; Seo, D.-K. Role of oxygen vacancies and Mn^{4+}/Mn^{3+} ratio in oxidation and dry reforming over cobalt-manganese spinel oxides. *Mol. Catal.* **2020**, *483*, 110704. [CrossRef]
41. Wang, W.L.; Meng, Q.; Xue, Y.; Weng, X.; Sun, P.; Wu, Z. Lanthanide perovskite catalysts for oxidation of chloroaromatics: Secondary pollution and modifications. *J. Catal.* **2018**, *366*, 213–222. [CrossRef]
42. Tang, W.; Li, W.; Li, D.; Liu, G.; Wu, X.; Chen, Y. Synergistic Effects in Porous Mn–Co Mixed Oxide Nanorods Enhance Catalytic Deep Oxidation of Benzene. *Catal. Lett.* **2014**, *144*, 1900–1910. [CrossRef]
43. Zhu, L.; Li, X.; Liu, Z.; Yao, L.; Yu, P.; Wei, P.; Xu, Y.; Jiang, X. High Catalytic Performance of Mn-Doped Ce-Zr Catalysts for Chlorobenzene Elimination. *Nanomaterials* **2019**, *9*, 675. [CrossRef]
44. Dravid, V.P.; Ravikumar, V.; Notis, M.R.; Lyman, C.E.; Dhalenne, G.; Revcolevschi, A. Stabilization of Cubic Zirconia with Manganese Oxide. *J. Am. Ceram. Soc.* **1994**, *77*, 2758–2762. [CrossRef]
45. Jiang, H.; Wang, C.; Wang, H.; Zhang, M. Synthesis of highly efficient MnO_x catalyst for low-temperature NH_3-SCR prepared from Mn-MOF-74 template. *Mater. Lett.* **2016**, *168*, 17–19. [CrossRef]
46. Cuervo, M.R.; Diaz, E.; de Rivas, B.; Lopez-Fonseca, R.; Ordonez, S.; Gutierrez-Ortiz, J.I. Inverse gas chromatography as a technique for the characterization of the performance of Mn/Zr mixed oxides as combustion catalysts. *J. Chromatogr. A* **2009**, *1216*, 7873–7881. [CrossRef] [PubMed]
47. Qin, Y.; Wang, H.; Dong, C.; Qu, Z. Evolution and enhancement of the oxygen cycle in the catalytic performance of total toluene oxidation over manganese-based catalysts. *J. Catal.* **2019**, *380*, 21–31. [CrossRef]
48. Li, L.; Wahab, M.A.; Li, H.; Zhang, H.; Deng, J.; Zhai, X.; Masud, M.K.; Hossain, M.S.A. Pt-Modulated $CuMnO_x$ Nanosheets as Catalysts for Toluene Oxidation. *ACS Appl. Nano Mater.* **2021**, *4*, 6637–6647. [CrossRef]
49. Mo, S.P.; Zhang, Q.; Li, J.Q.; Sun, Y.H.; Ren, Q.M.; Zou, S.B.; Zhang, Q.; Lu, J.H.; Fu, M.L.; Mo, D.Q.; et al. Highly efficient mesoporous MnO_2 catalysts for the total toluene oxidation: Oxygen-Vacancy defect engineering and involved intermediates using in situ DRIFTS. *Appl. Catal. B Environ.* **2020**, *264*, 118464. [CrossRef]
50. Zhou, C.; Zhang, H.; Zhang, Z.; Li, L. Improved reactivity for toluene oxidation on MnO_x/CeO_2-ZrO_2 catalyst by the synthesis of cubic-tetragonal interfaces. *Appl. Surf. Sci.* **2021**, *539*, 148188. [CrossRef]